Geomechanics and Engineering, *Vol. 32, No. 4 (2023) 397-409*
https://doi.org/10.12989/gae.2023.32.4.397

An assessment of non-linear elastic and elasto-plastic analyses with regards to tubular steel piles embedded in sands

Adolfo Foriero* and Zeinab Bayati[a]

Department of Civil and Water Engineering, Université Laval, Québec, Canada

(*Received June 16, 2020, Revised January 13, 2023, Accepted January 20, 2023*)

Abstract. This study examines two traditional approaches (non-linear elastic and elasto-plastic) in association with 2D and 3D FEM analyses of a box-section pile embedded in sand. A particular emphasis is placed on stress singularities concerning both re-entrant corners of the pile section and the resulting tension zones. From the experience gained in this study, non-linear elastic soil models are less restrictive when one considers stress singularities and their possible effects on convergence of the solution. At least for monotonic loading, when compared with field tests, non-linear elastic models yield better results than the plasticity ones. On the other hand, although elasto-plastic models are not limited to monotonic loading, they are much more sensitive to stress singularities. For this reason, a spherical elastic region is necessary at the pile tip to ensure convergence. Without this region, one must artificially impose an apparent cohesion to limit the tension stresses within a sand medium.

Keywords: elasto-plastic soil models; long-term failure analysis; non-linear elastic soil models; sandy soils; stress singularities; tubular steel piles

1. Introduction

In a previous paper, the authors, Foriero and Bayati (2018), considered the three-dimensional buckling behavior of a steel box-section pile embedded in typical soils. That study examined the suitability of the pile section with regard to buckling, bearing in mind the influence of the surrounding elastic soil-medium. It was demonstrated that the critical buckling load increases as the lateral resistance of the surrounding soil medium increases. This finding was also reported by Shields (2007) and El Kamash and El Naggar (2018). In general, increasing the relative density of the surrounding soil increases the buckling resistance of pile (Zhang *et al.* 2020).

The buckling axial load of slender piles is smaller than that of short piles. However, for piles embedded in soft soils, the difference becomes negligible (Ramirez-Henao and Paul Smith-Pardo 2015). Long slender piles are susceptible to buckling failure under large axial loads. The lateral movement of soil, because of pile buckling, implicates a soil reaction dependent on the pile deformation. In addition, the pile movement is restrained by the surrounding soil. As a result, the pile buckling is fundamentally affected by the pile-soil interaction (Deng *et al.* 2016).

The main causes of failure of long piles are: (1) inadequate strength of pile section upon eccentric axial or lateral loads and geometric imperfections, or (2) the loss of soil bearing capacity, leading to pile buckling or material yielding (Tomlinson and Woodward 2014). The effect of geometric imperfections (manifested in initially bent piles) on the load-bearing capacity of axially loaded piles has been widely studied (Glick 1948, Broms 1963, Rezaiee and Mazindrani 1990, Dunlop *et al.* 1993, Kumar Khan and Pise 1997, Paik *et al.* 2011, Nadeem *et al.* 2015). It was observed that the axial load-carrying capacity decreases in piles with initial curvature compared with straight piles. The load-bearing capacity of piles embedded in both granular and cohesive soils has been investigated in numerous studies (Eslami and Fellenius 1997, Veiskarami *et al.* 2011, Ren *et al.* 2014, Hataf and Shafaghat 2015, Jeong *et al.* 2015, Alielahi and Adampira 2016). The surrounding soil conditions play a significant role in the analysis and design of piles due to the inherent uncertainties of soil properties. Accordingly, Soil-Structure Interaction (SSI) problems are complicated, particularly when designing slender piles. Once design of the pile section satisfies stability with respect to buckling, then the next step verifies that the pile-soil system as a whole does not fail. Consequently, one verifies against foundation failure using either a non-linear elastic or a plasticity approach for the surrounding soil medium. The pile section may change in shape at some time during the life of the supported structure, and because of the non-linear nature of the soil medium, the pile-soil system may fail. However, in general, the possibility of foundation failure is related to both the changes in shape of the pile section and the non-linear nature of the supporting soil. A recent example of this type of significant foundation issue is the 197-meter-tall Millennium Tower in San Francisco. Since completion of construction in 2008, soil liquefaction produced piles section changes resulting in the sinking (0.44 m) and tilting (0.36 m northwest) of the high-rise 58-story building. Moreover, the Millennium tower rests on a liquefiable soil

*Corresponding author, Associate Professor
E-mail: Adolfo.Foriero@gci.ulaval.ca
[a]Ph.D.

ISSN: 2005-307X (Print), 2092-6219 (Online)

deposit, and because the San Francisco region is at high risk for earthquakes, the problem of the excessive deformation of piles is serious. More common section changes are related to the low cycle fatigue strength of steel piles (Dusicka *et al*. 2007). Not to mention other construction related imperfections that can result in the initial deformations of the pile sections.

Thus, in this study, the authors examine the possibility of foundation failure by considering large strains of the surrounding soil. This means encapsulating the pile-soil system behavior and verifying that the previously chosen pile section (stable with respect to buckling) and surrounding soil provide a united stable foundation.

In classical soil mechanics verification of the stability and serviceability of the foundation involved two independent steps (Wood 2007). Here, one achieves this goal by considering 2D and 3D FEM analyses that incorporate realistic soil properties and classical soil models. This paper presents a critical view of these approaches, delving on the possible problems one encounters during the FEM analyses.

This study considers classical soil models for sands. In more general terms, these models are appropriate for granular soils, when considering long-term analysis (drained conditions). In the literature, use of hyperbolic soil models (Kondner 1963, Duncan and Chang 1970, Hardin and Drnevich 1972, Fahey and Carter 1993) prevail when one wishes to describe the nonlinear stress-strain behavior of such soils. For example, Desai (1974) used the Duncan-Chang hyperbolic soil model for the finite element analysis of piles in sands. Emphasis on the importance of considering the soil nonlinearity via finite element analysis was brought forth by Cheung *et al.* (1991). In that study, the Duncan-Chang constitutive model served as the basis of the computed pile load-settlement curves. Results of the simulations were compared with field measurements of a static pile axial load test. The satisfactory agreement of the simulation with the test results demonstrated that using a soil nonlinear elastic model is a valid alternative to describe a realistic stress-strain behavior of the soil medium.

The Drucker-Prager (Drucker and Prager 1952) and Mohr-Coulomb (Heyman 1972) constitutive plasticity models were utilized in numerous studies (Trochanis *et al*. 1991, Lee and Salgado 1999, Jesmani *et al.* 2014, Nadeem *et al.* 2015, El Kamash and El Naggar 2018, Bakroon *et al.* 2019) owing to their relative simplicity to model the soil surrounding the pile. These two pressure dependent models adjust to the particulate nature of a soil medium. These soil behavior models were also chosen because of their acceptance and widespread use in geotechnical engineering. Such models are generally more appropriate when considering cemented materials.

In this paper, two- and three-dimensional nonlinear finite element analyses of a steel box-section pile partially embedded in a sandy soil medium are considered. Steel box-section piles have important applications. For example, they can be conveniently introduced into a wall of standard sheet piles at any point where heavy loads are applied. They can be used to resist vertical and horizontal forces and can generally be positioned in the wall such that its aesthetical appearance is unaffected. Boxes may also be used as individual bearing piles for foundations or in open jetty and dolphin construction, and can be driven into natural soil deposits such as clays, silts and sands, very compact ground, and soft rocks.

The pile steel box section is considered to behave linear-elastically, and the embedded end of pile is modeled as free. The FEM analyses consider the stability of the pile-soil system after the pile experiences some perturbation in shape being an imposed fixed horizontal displacement of the pile head. Details of the FEM modelling encompassing these facts are given at a later section. Consideration of initial stresses is essential for the nonlinear analysis of soil-structure interaction problems. In the present study, the initial soil stresses employed in the first step of analysis are related to the state prior to the pile installation, e.g., calculated using the average soil density. However, some previous studies performed with the finite element analysis method used the horizontal stresses of the soil at failure as the initial horizontal stresses. These horizontal stresses were back calculated from the results of the field loading tests (Desai and Holloway 1972, Desai 1974). The effects of soil plasticity and slippage between pile and soil was investigated in a parametric study of the response of single piles subjected to axial loads by Trochanis *et al.* (1991). Finite element analysis of the soil behavior was performed using the Drucker-Prager plasticity criterion; while piles were modeled as linearly elastic material. The study showed that the pile-soil slippage is a significant source of nonlinear behavior and energy dissipation under axial loading and emphasized the necessity of accurately modeling the interface elements between pile and soil.

Studies on axially loaded piles having a steel box cross-section, embedded in non-linear or elasto-plastic soil mediums, are scarce. For this reason, it is important to mention research studies that are somewhat associated because of their field tests. These field tests are used to verify the soil model investigated in the present study. One of these is the study of Comodromos *et al*. (2003). In that study, the researchers present the results of a reinforced concrete pile embedded in a multi-layered soil medium including clayey and sandy layers. The study also included analyses of pile groups in order to investigate pile-group effects. A typical pile group was constituted by one compression pile surrounded by different numbers of tension piles. A three-dimensional finite difference nonlinear model was developed to simulate a static axial load test. The results showed that the interaction between the compression and reaction piles affect the overall load-settlement curve of the compression pile. Finite difference simulations of a single pile yielded a higher load-settlement curve when compared to that of the pile within the pile-group (demonstrating group efficiency). Another study is that of Comodromos *et al*. (2009), where they investigated the behavior of a pile raft foundation under vertical and lateral static load tests and compared it with a three-dimensional FEM nonlinear analysis. A pile foundation design method was then proposed by considering the contribution of the raft. It was also shown that the most significant parameter affecting the load distribution is the

Table 1 Elastic properties of pile material and soil medium

	E_s (MPa)	ν
Soil (Dense Sand)	60	0.3
Pile (ASTM-A36 Structural Steel)	200e3	0.33

pile-interaction with the group.

2. Considering the FEM Model

Two different classical point of views were followed in the present study in order to model the soil medium. One is the non-linear elastic approach characterized by the Duncan-Chang and Hyperbolic models. The other is the plasticity approach via the Drucker-Prager and Mohr-Coulomb models. For the FEM analyses, the imposed kinematic boundary condition consists of an initial horizontal perturbation of 20 mm imposed on the pile head. The pile head is then subject to step vertical incremental loads. This type of analysis is suited for both non-linear elastic and plasticity models. All of the plasticity simulations in this study were carried out using an associative flow rule. The elastic properties of pile material and soil medium (Young Modulus (E_s) and Poisson's Ratio (ν)) used in the finite element analyses are shown in Table 1.

Thin layer elastic interface elements were selected in order to model the interface condition between the pile surface and the soil. These types of interface elements allow for the possibility of an infinitely normal and imposed tangential stiffness. Thus, simulations considered the perfectly rough and intermediate cases of roughness via the tangential stiffness of the interface elements.

The boundary conditions set for the FEM mesh surrounding the soil are rollers. This type of boundary condition is preferred over the fixed boundary condition because the finite element domain should be given as much as freedom as possible, just as in nature. However, this is not critical because after several trial simulations the boundary was placed far enough such that even a fixed boundary will not affect the results. The bottom soil has also been restrained using a fixed boundary condition with the same reasoning implying a deep enough boundary. In all the simulations, no assumptions of fixity of the pile tip were imposed. In other words, the pile tip is modelled to be free of movement or completely unrestrained.

A typical 3D finite element mesh is constituted with tetrahedral elements, totaling 651219 degrees of freedom. Simulations involving load control for non-linear elastic analyses amounted to approximately 2 hours of C.P.U., whereas for the plasticity analyses this amounted to 5 hours C.P.U.

2.1 Singularities in FEM model

In all simulations of this study, the finite element model experiences singularities — points where the stresses tend toward an infinite value. These stress peaks are expected because of the various effects of modeling. Such stresses are less of a problem when one considers the soil as non-linear elastic medium. However, a convergence issue arises for plasticity models when those stress peaks exceed the yield stress by a considerable amount (Sönnerlind 2015). For a channel-sectioned pile, sharp re-entrant corners at the pile surface and particularly at the tip, will cause a singularity in the derivatives of the dependent or secondary variables such as the stresses. Consequently, the strains can become unbounded since the essential conditions or the degrees of freedom are the displacements. The material model must limit this effect in order to prevent the stresses from becoming infinite.

An infinitely stiff sand medium supporting a pile does not really exist. Elasticity models alone assume this. If now one uses an elasto-plastic approach involving the Drucker-Prager or Mohr-Coulomb plasticity models, then a singularity caused by tension zones in the nearby boundary condition arises, and is not acceptable. Remedies to this condition are possible. An increase of finite elements in these zones (sharp corners) might not be useful. In fact, the smaller the elements that are used in these corners, the higher the values of stress that will be found. The results will not converge since the true solution tends toward an infinite value. Since sharp corners are a reality in the present context, one of the remedies used in this study is to enclose the singularity in a small elastic domain. Ultimately, one also needs to limit the tension produced by the elastic portion of the model. These points will be addressed in the next sections of the paper.

3. FEM results for non-linear elastic modelling of pile-soil system

In this section of the study, two non-linear elastic models are adopted for the FEM study of the pile-soil system. These are respectively the hyperbolic and Duncan-Chang nonlinear models. The hyperbolic model is characterized by the following secant modulus expression

$$G_s = \frac{G}{1+\left(\frac{\gamma}{\gamma_{ref}}\right)^n} \tag{1}$$

Where the variables Gs, G, γ, γ_{ref} and n are respectively the secant shear modulus, the initial or maximum shear modulus (at zero shear strain), the shear strain, a reference shear strain (a shape-control strain) and a strain exponent n. The secant modulus is computed iteratively in the FEM analyses for the rendering of:

$$\tau = G_s \gamma \tag{2}$$

Where, τ and γ are respectively the shear stress and strain. A typical example of the above equations used in the FEM analyses are given in Fig. 1.

As seen in the figure, the secant modulus drops off, indicating that the stiffness of the sand decreases as the shear stress increases. The utility of such a model is two-

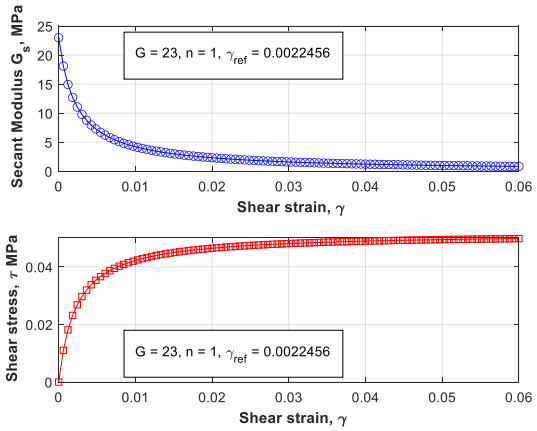

Fig. 1 Secant shear modulus and shear stress vs. shear strain for Hyperbolic nonlinear elastic model

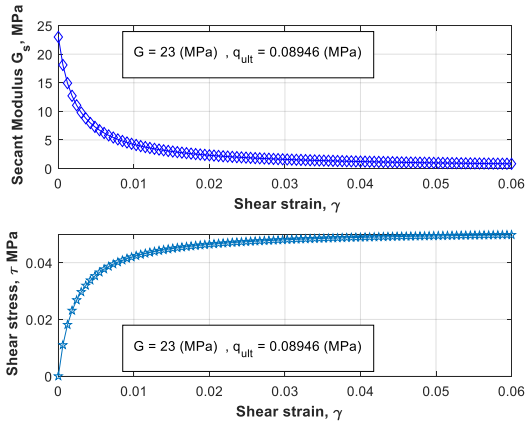

Fig. 2 Secant shear modulus and shear stress vs. shear strain for Duncan-Chang nonlinear elastic model

fold: (1) not only is the model necessary in the calculation of the shear stress-strain response but (2) the model is detrimental in detecting the plausible failure condition. From here on, the failure condition is defined as a constant shear stress at the start of an unlimited shear strain. This complies with the critical state theory generally used in soil mechanics.

The Duncan-Chang model uses a similar expression. This model is given as

$$G_s = \frac{G}{1+\frac{G}{q_{ult}}\sqrt{3}\gamma} \tag{3}$$

Where again the variables G_s, G, and γ are respectively the secant shear modulus, the initial or maximum shear modulus (at zero shear strain) and the shear strain. As for the variable q_{ult}, in the above equation, it is generally calculated with the expression involving the principal stresses via $q_{ult} = (\sigma_1' - \sigma_3')_{ult}$. The principal stresses for a sand deposit are generally calculated using the unit weight and the friction angle ($\sigma_1' = \gamma' z\,, \sigma_3' = K_o^{nc}\sigma_1'$), depending if it is in a loose ($K_o^{nc} = 1 - \sin(\varphi_{cr}')$); (Jaky 1944) or dense state ($K_o^{oc} = K_o^{nc}(OCR)^p$); (Meyerhof 1976). This in turn requires the calculation of the over-consolidation ratio (OCR) and an empirical parameter p usually taken as 0.5. For the purposes of obtaining the same secant modulus expression as the hyperbolic model (with $n = 1$), one can calculate an equivalent Duncan-Chang secant modulus by letting $q_{ult} = G\sqrt{3}\gamma_{ref}$. A confirmation of this is shown in Fig. 2.

Such models are used quite extensively in geotechnical engineering (Kondner 1963, Duncan and Chang 1970) to model sand deposits. The first advantage these models have over plasticity models (covered in the next section) is the fact that convergence issues are independent of the level of tension produced by the elastic components. This is a significant advantage because the effect of singularities, such as those mentioned in the last section, become less critical.

In the present study, these models are used in 2D, then 3D FEM analyses to study the stability of a soil-pile system when the pile shape is initially perturbed. As previously mentioned, the driving boundary condition covered is the case of an initial horizontal displacement and incremental vertical pile head loading. At this stage, an explanation of the FEM simulations is warranted. This type of FEM analyses considers the stability of the pile-soil system after the pile experiences some perturbation in shape. In the subsequent FEM simulations, this perturbation is an imposed fixed horizontal displacement of the pile head. In a previous paper, the authors (Foriero and Bayati 2018) established the critical buckling loads for the pile section while considering the surrounding sand medium as elastic. In the present scenario, the problem takes place before the pile section buckles. Specifically, the pile section changes in shape at some time during the life of the supporting structure, and because of the non-linear nature of the sand medium, the soil-pile system may fail (instability in the present context).

A non-linear elastic FEM analysis in COMSOL software requires the input of the elastic parameters of both the soil medium and pile, as well as the parameters corresponding to the models alluded to in Eqs. (1) and (3). These parameters are given in Tables 2 and 3. The geometrical dimensions of the pile section were selected to comply with the standard Canadian Steel Section Properties derived from

Table 2 Duncan-Chang Model parameters

Bulk modulus K (MPa)	G (MPa)	Ultimate deviatoric stress q_{ult} (MPa)
50	23	0.08946

Table 3 Hyperbolic Model parameters

K (MPa)	G (MPa)	n	γ_{ref}
50	23	1.0	0.002246

Table 4 Geometric properties of pile section

Diameter D (mm)	Thickness (mm)	Unsupported length (m)	Total length L (m)	Slenderness (L/D)
305	16	2.0	8.0	26.23

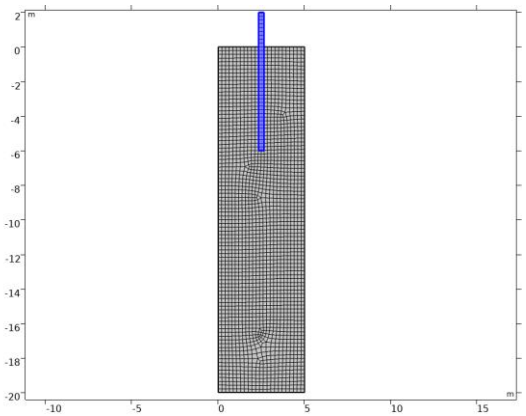

Fig. 3 2D finite element meshed model of the pile-soil system used in simulations

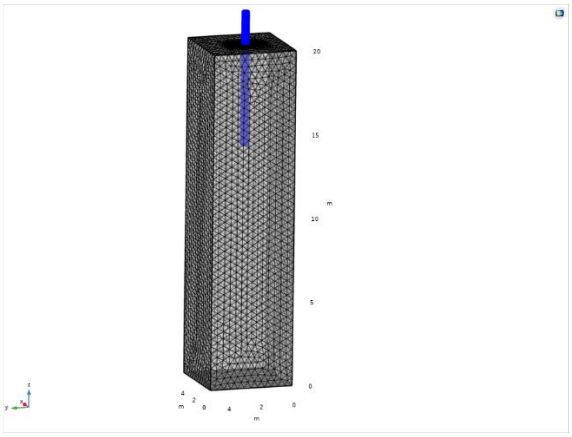

Fig. 4 3D finite element meshed model of the pile-soil system used in simulations

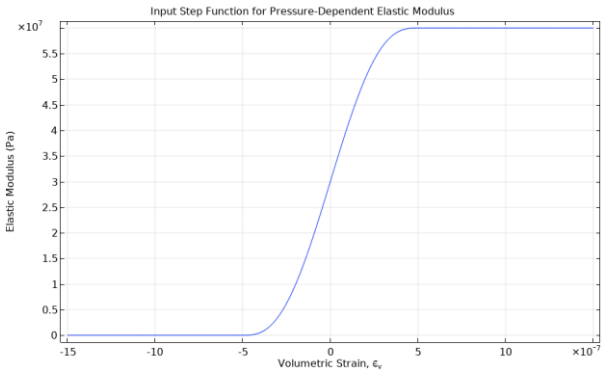

Fig. 5 The elastic modulus input function used in the geostatic analyses

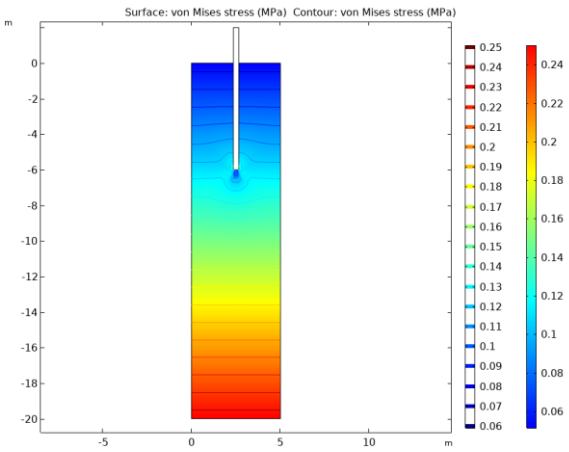

Fig. 6 The von Mises stress contours resulting from the FEM 2D geostatic analysis using the pressure dependent elastic modulus

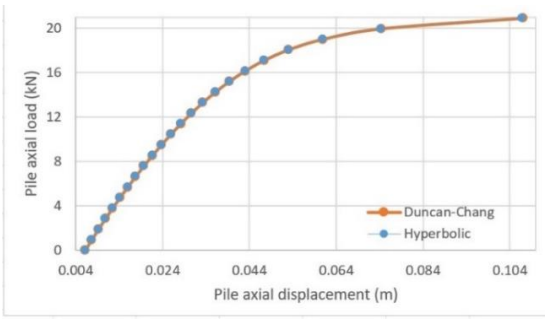

Fig. 7 Comparison of pile axial load-axial displacement graphs for 2D FEM analysis using Duncan-Chang and Hyperbolic models

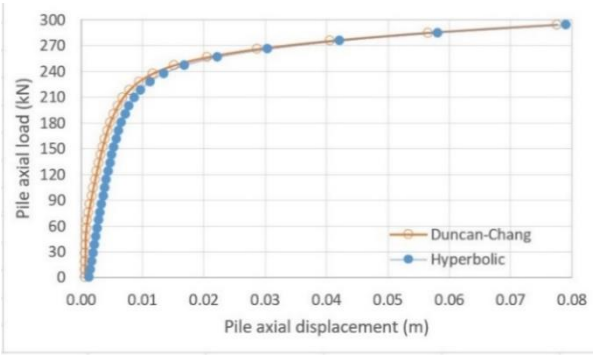

Fig. 8 Comparison of pile axial load-axial displacement graphs for 3D FEM analysis using Duncan-Chang and Hyperbolic models

CISC SST9.2 from the ninth edition of the Canadian Steel Handbook (CISC 2007). These geometric values are given in Table 4, while the extent of the finite element models is shown by the FEM meshes of Figs. 3 and 4.

The first step of finite element simulations begins with a geostatic analysis, in order to establish the initial stress field of the pile-soil system. Furthermore, to reduce the effect of tension (because of elasticity theory) a pressure dependant elastic modulus is convenient. In COMSOL, this is achieved by defining an elastic modulus as a step function having a positive low value at negative pressures. Fig. 5 illustrates the input function used in the geostatic analyses. One cannot overemphasize that a pressure dependant elastic modulus is used only in the geostatic analyses. Fig. 6 depicts the FEM results of the von Mises stress contours resulting from the geostatic analysis using the pressure dependant modulus of Fig. 5.

The second step of the analyses involves the pile head loading of the perturbed pile section. As previously mentioned, the perturbed pile is modeled by imposing a finite horizontal translation of the pile head. The imposed loading of the pile head is achieved with a series of static

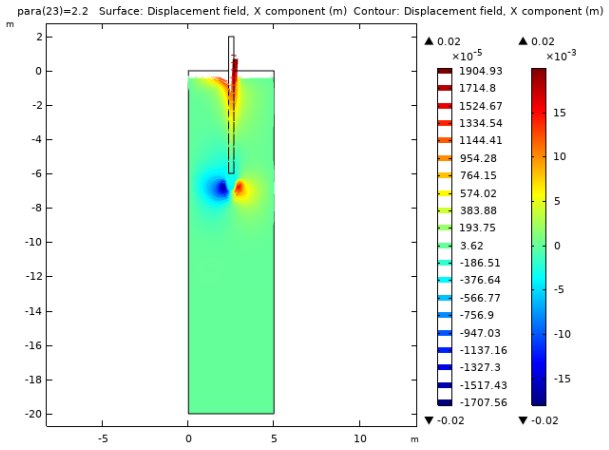

Fig. 9 2D FEM analysis results of horizontal displacements for a maximum vertical pile head load of 20.9 kN (equivalent to 2200 kPa of axial pressure) using Duncan-Chang model

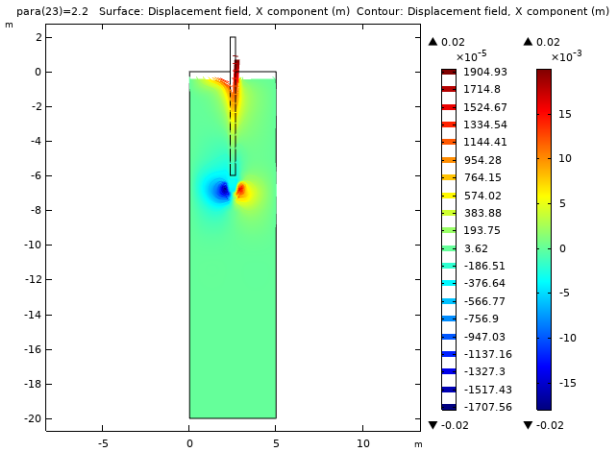

Fig. 10 2D FEM analysis results of horizontal displacements for a maximum vertical pile head load of 20.9 kN (equivalent to 2200 kPa of axial pressure) using Hyperbolic model

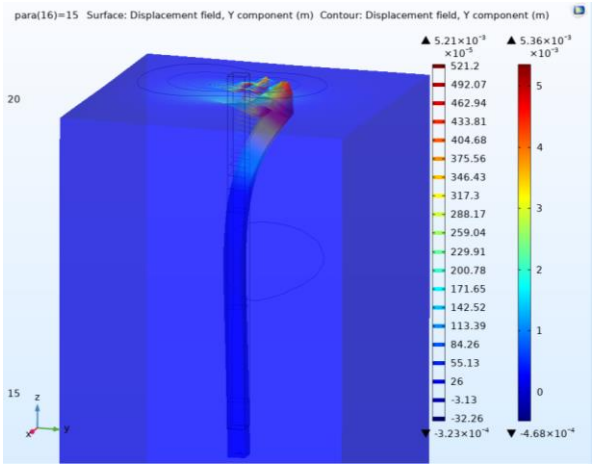

Fig. 11 3D FEM analysis results of lateral soil displacements for the failure vertical pile head load of 294.6 kN (equivalent to 15000 kPa of axial pressure) using Duncan-Chang model

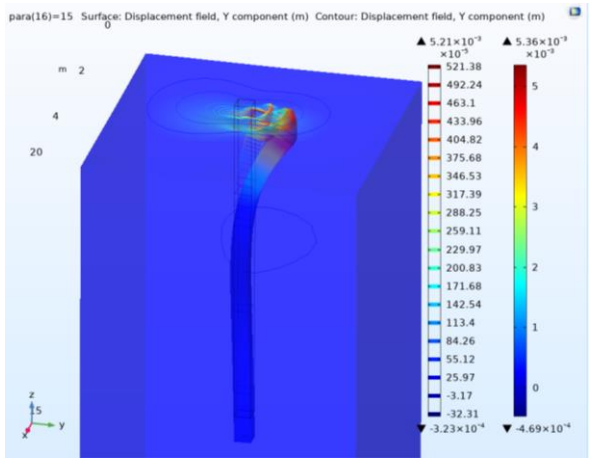

Fig. 12 3D FEM analysis results of lateral soil displacements for the failure vertical pile head load of 294.6 kN (equivalent to 15000 kPa of axial pressure) using Hyperbolic model

monotonic vertical load increments. For comparison with FEM simulations, that consider plasticity models (covered in the next section of this paper), a uniform vertical pressure of 90 (kPa) is applied at the level of the ground surface.

This uniform pressure was necessary in order to remove the tensile stresses produced by elasticity which otherwise would be unrealistic. In fact, sand is unable to resist tension unless it is cemented and consequently this measure limits the high tensile stresses particularly at the ground surface. Typical 2-D and 3-D FEM results, using the above constitutive models with the initial stress field of Fig. 6, are discussed next. Fig. 7 depicts the results of typical 2D FEM simulations of pile axial load versus axial displacement using the Duncan-Chang and Hyperbolic models. One observes the difference is imperceptible between the results of simulations using these two models. Both the behaviors prior to failure and at failure are similar. However, for the 3-D FEM simulations, as shown in Fig. 8, the behavior prior to failure is slightly different.

As mentioned previously, the driving mechanism for these results is a monotonically increasing vertical load and a horizontal displacement of 20 mm applied at the pile head. Figs. 9 and 10 depict the horizontal displacements at the maximum load attained by the non-linear analyses with the respective Duncan-Chang and Hyperbolic models.

It is clear from the figures that a tension zone develops at the pile tip in the lower surrounding sand. This is evidently caused by elasticity theory. One deduces from the previous figures, that a non-linear elastic analysis brings forth certain limitations. The first and most obvious one is related to the tension zones produced as a result of elasticity. This requires a certain degree of judgement on the part of the engineer. It must be said that non-linear elasticity and in particular the Duncan-Chang and Hyperbolic models, have been used for decades in geotechnical engineering. These non-linear models when used in a 3D FEM analysis yield a clearer picture of the surrounding soil displacements. This is shown in Figs. 11 and 12 pertaining again respectively to the Duncan-Chang and Hyperbolic models. In these figures, only the horizontal soil

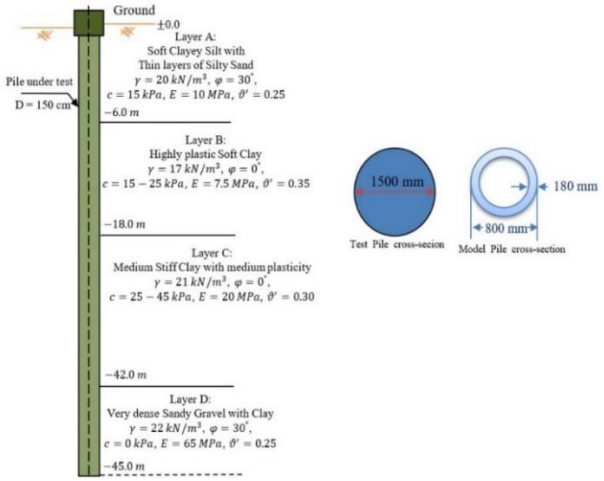

Fig. 13 Details of soil profile and test pile used in Comodromos *et al.* (2003) study along with the soil conditions and model pile used in FEM analyses

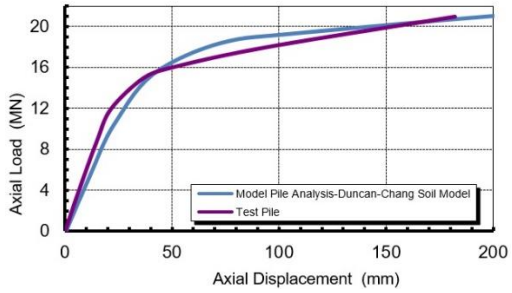

Fig. 14 Comparison of the results of the test pile (Comodromos *et al.* 2003) and the results of the FEM analysis using the Duncan-Chang model

displacements are shown. One observes that the horizontal soil displacements are located primarily in the upper region of the pile-soil system. Moreover, for both models, the FEM simulations yield a soil pile-up at the ground surface.

4. Validation of nonlinear elastic analyses using field tests

It is always desirable to confirm the applicability of an FEM model to a completely independent study. A field study on reinforced concrete piles by Comodromos *et al.* (2003) is considered in this section of the present study. Fig. 13 gives a description of the test pile as well as the soil conditions covered in that study. Since the present study deals with a tubular cross section, a modular transformation was required for the FEM simulations. This is shown in Table 5 along with the properties of the test and model pile.

The non-linear FEM simulations, in these particular analyses follow the load-control procedure of the field test. Tables 6 and 7 show the soil non-linear elastic parameters used in the simulations. Figs. 14 and 15 demonstrate that the Duncan-Chang and Hyperbolic models are quite effective in yielding the axial load versus displacement curve of the field test. This is even more so when one considers the approximate nature of the field soil properties.

Table 5 Properties of the test pile used in Comodromos *et al.* (2003) study and the model pile used in FEM analyses

Section properties	Test Pile	Model Pile
Material	Reinforced Concrete (C30/35), 45 steel bars (25 mm of diameter): (Asteel = 0.0318 m^2 = $\frac{1}{55}A_{section}$)	Steel
E (GPa)	42	210
Diameter (mm)	1500	External: 800 Internal: 440
Cross-sectional area (m^2)	1.77	0.35

(Modular ratio = $\frac{E_{Reinforced\ Concrete}}{E_{steel}} = \frac{42\ Gpa}{210\ Gpa} = 0.2$)

Table 6 Duncan-Chang model parameters used in the FEM analyses using the model pile

	K (MPa)	G (MPa)	q_{ult} (MPa)
Layer A	6.7	4.0	0.018
Layer B	8.3	2.8	0.05
Layer C	16.7	7.7	0.1
Layer D	43.3	26.0	0.71

Table 7 Hyperbolic model parameters used in the FEM analyses using the model pile

	K (MPa)	G (MPa)	n	γ_{ref}
Layer A	6.7	4.0	1.0	0.025
Layer B	8.3	2.8	1.0	0.011
Layer C	16.7	7.7	1.0	0.007
Layer D	43.3	26.0	1.0	0.016

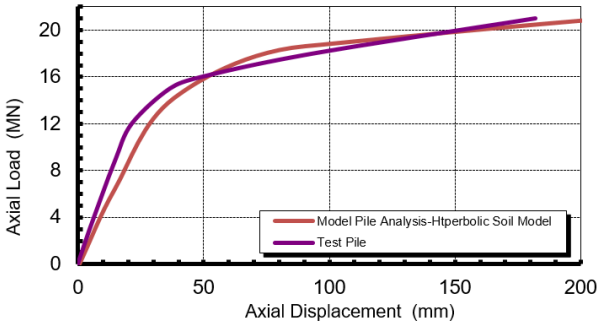

Fig. 15 Comparison of the results of the test pile (Comodromos *et al.* 2003) and the results of the FEM analysis using the Hyperbolic model

Consequently, both the non-linear Duncan-Chang and Hyperbolic models are quite effective in modelling piles in sand under monotonic loading.

5. Elasto-plastic analyses

This section of the paper considers the elasto-plastic stress analyses of the problem in 2D and 3D. The analyses consider two different plasticity behaviors via the Mohr-

Coulomb and Drucker-Prager criteria. Generally, plasticity theory is formulated by considering three requirements: First, a relationship between stress and strain must be formulated to describe material behavior under elastic conditions. Second, one must specify a yield criterion indicating the stress level at which plastic flow initiates. Finally, a relationship between stress and strain must be developed for post-yield behavior.

In FEM programs, the stress level is monitored and compared to the level of the yield stress. For the Mohr-Coulomb yield criterion, the stress level measurement is generally taken as (Owen and Hinton 1986, Foriero 2004, Foriero and Ladanyi 1995, Foriero and Ladanyi 1991, Foriero and Ladanyi 1990).

$$\sigma^{level} = \frac{1}{3} J_1 \sin(\phi') + (J_2')^{\frac{1}{2}} \left(\cos(\theta) - \frac{1}{\sqrt{3}} \sin(\theta) \sin(\phi') \right) \quad (4)$$

where J_1, J_2', θ and φ' are respectively the first stress invariant $J_1 = \sigma_{ii} (1 \le i \le 3)$, the second deviatoric stress invariant $(J_2' = \sigma_{ij}' \sigma_{ij}',\ \sigma_{ij}' = \sigma_{ij} - \delta_{ij}\sigma_{kk}, (1 \le i, j, k \le 3))$, the angle of internal friction of the soil medium and the Lode angle obtained with

$$\sin(3\theta) = -\frac{3\sqrt{3}}{2} \frac{J_3}{(J_2')^{\frac{3}{2}}},\ J_3 = \frac{1}{3} \sigma_{ij} \sigma_{jk} \sigma_{ki} (1 \le i, j, k \le 3) \quad (5)$$

Whether or not plastic deformation takes place at any point is governed by the previous stress level (4). For plastic flow to occur, this stress level must achieve the equivalent yield stress

$$\sigma_Y = c \cos(\phi') \quad (6)$$

where c represents an apparent cohesion. There are objections to this yield stress (5). First, full mobilisation of the cohesion c and friction angle φ' does not occur at the same time and consequently for design purposes, to be on the safe side, one neglects the c component (Budhu 2010). Second, for granular sand material $c = 0$ and thus $\sigma_Y = 0$.

This leads to numerical instabilities, which will be discussed shortly. For the Drucker-Prager yield criterion, which is a modification of the previous Mohr-Coulomb criterion, the stress level is

$$\sigma^{level} = \alpha J_1 + (J_2')^{\frac{1}{2}} \quad (7)$$

where α is given as

$$\alpha = \frac{2\sin(\phi')}{\sqrt{3}(3 - \sin(\phi'))} \quad (8)$$

The equivalent yield stress in this case is

$$\sigma_Y = \frac{6 \cdot c \cdot \cos(\phi')}{\sqrt{3}(3 - \sin(\phi'))} \quad (9)$$

The same objectionable remarks as for the Mohr-Coulomb criterion apply here. Commercially available FEM programs such as COMSOL protect their code and consequently it is difficult to interpret explicitly the algorithm used. Moreover, commercial programs upgrade their codes frequently. However, based on intuition and experience, the residual forces during any particular iteration are expressed as

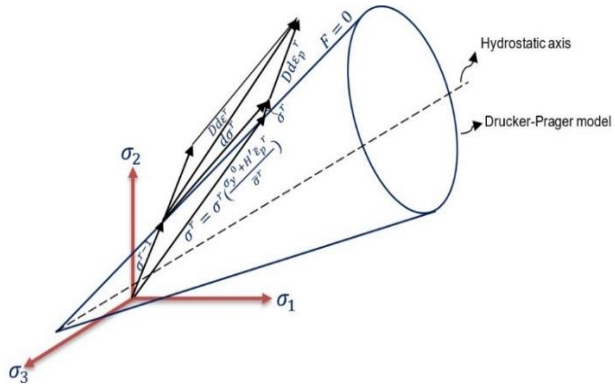

Fig. 16 Incremental stress change at a Gauss point that has previously yielded

$$\psi(\phi^r) = -J(\phi^r) \Delta\phi^r \quad (10)$$

Where

$$\{\psi\} = \left(-\frac{\partial}{\partial\varphi_1}(H)\{\varphi\}, \ldots, -\frac{\partial}{\partial\varphi_{n-1}}(H)\{\varphi\}, -\frac{\partial}{\partial\varphi_n}(H)\{\varphi\} \right) . \{\Delta\varphi^r\} - [H]\{\Delta\varphi^r\}$$

$$H = \begin{bmatrix} h_{1,1} \ldots\ldots\ldots h_{1,n} \\ h_{2,1} \ldots\ldots\ldots h_{2,n} \\ \vdots\ \vdots\ \vdots\ \vdots\ \vdots \\ \vdots\ \vdots\ \vdots\ \vdots\ \vdots \\ h_{n,1} \ldots\ldots\ldots h_{n,n} \end{bmatrix} \quad (11)$$

In other words

$$\Delta\phi^r = -\left[H(\phi^r) + H'(\phi^r) \right]^{-1} \cdot \psi(\phi^r) \quad (12)$$

Generally, the applied loads for the rth iteration are the residual forces ψ^{r-1} calculated at the end of the (r-1)th iteration. These applied loads give rise to the displacements increments $\Delta\varphi^r$ and consequently the strain increments, $\Delta\varepsilon$. FEM algorithms consider whether or not yielding took place at the Gauss point during the (r-1)th iteration. Therefore, they verify if $\bar{\sigma}^{r-1} > \sigma_Y = \sigma_Y^o + H' \bar{\varepsilon}_p^{r-1}$, where $\bar{\sigma}^{r-1}$ is the σ^{level} given in Eqs. (4) and (7), and σ_Y is the yield stress of Eqs. (6) and (9). Here H' is a strain hardening parameter and $\bar{\varepsilon}_p^{r-1}$ is the effective plastic strain at the rth iteration. If this condition is true, then the algorithm must consider whether or not the Gauss point has previously yielded. If the Gauss point was not previously yielded then that means the Gauss point is unloading elastically. If on the other hand, the Gauss point was previously yielded and the stress is still increasing, then the excess stress must be reduced to the yield surface as shown in Fig. 16. On the other hand, if the condition is false, which implies that the Gauss point had not previously yielded, then the Gauss point is still elastic. If the Gauss point has yielded during the application of the load, then again the portion of the stress greater, then the yield value must be reduced to the yield surface Fig. 17.

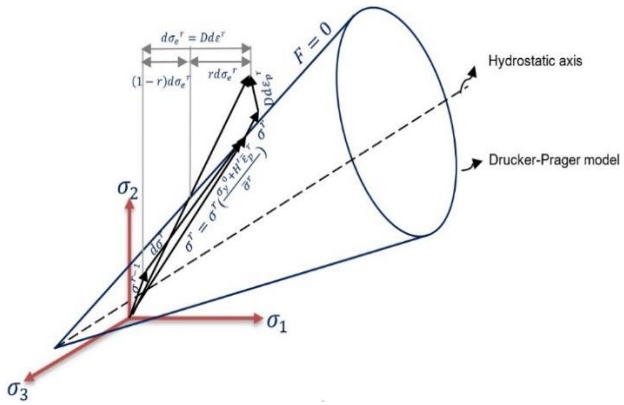

Fig. 17 Incremental stress change at a point in an elasto-plastic continuum at initial yield

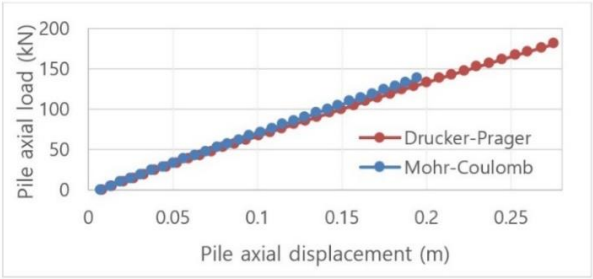

Fig. 18 Pile head axial load vs. axial displacement from the 2D load-control FEM plasticity analysis

The discussion mentioned above is standard practice. There are, however, some variations in FEM commercial codes in order to speed up the calculations and convergence. Convergence is monitored locally at each node according to displacement changes that occur during any particular iteration r by way of

$$\frac{\left|\Delta d^{r}\right|}{\left|d^{1}\right|}\times 100 \le TOLER \tag{13}$$

where d^1 is the elastic displacement occurring upon application of the load increment and Δd^r is the change in nodal displacement during the rth iteration. Convergence considering displacements is severe and consequently very sensitive to the singularities previously mentioned.

6. Discussion of FEM plasticity analyses

This section presents a critical discussion of the Mohr-Coulomb and Drucker-Prager models in the context of plasticity analysis. A consideration of both 2D and 3D FEM results permits a better understanding of the implicit numerical difficulties encountered. Again, as per the non-linear elastic analyses, the problem of singularities remains. Numerous attempts at obtaining a converged solution lead to a new modelling strategy in order to eliminate these singularities. The solution is the introduction of a spherical elastic zone in the immediate vicinity of the pile tip. This elastic zone is necessary because of the extremely high stresses induced by the corners of the pile tip, these stresses becoming intangible, as the mesh is refined. Remarkably, this rigid zone at the pile tip is justifiable. In fact, geotechnical engineers, in a plethora of articles (Budhu 2007), assume such rigid wedges at the bottom of footings as well as pile tips. Laboratory tests do confirm the existence of such rigid wedges (Al-Soudani and Albusoda 2021). The compaction of the soil at the pile tip, where stresses are extremely high, produces a very stiff zone. Practically this zone is elastic and surrounded by an elastic-plastic domain. This implies imposition of a radius equal to the pile diameter in the ensuing elastic-plastic analyses of the Mohr-Coulomb and Drucker-Prager models. This approach reduces the convergence issues and mesh refinement was possible.

Numerous FEM simulations in both 2D and 3D enabled the study of the influence of this spherical elastic zone. One cannot overemphasize that failure loads were obtained with different values of cohesion and friction angle for the elastic-plastic analyses using both the Drucker-Prager and Mohr-Coulomb failure criteria. The cohesion is necessary in the COMSOL in order to limit tension stresses. In fact, granular soils in general do not possess cohesion except for what in the field is called “apparent cohesion”. Apparent cohesion is made up of three components: electro-chemical surface forces, unsaturated suction and cementation. Although in this study, no apparent cohesion is assumed and an artificial cohesion is imposed to limit tension. This is a method used in many of COMSOL modelling examples. Figs. 18 and 19 (a and b) compare the axial pile load versus pile head displacements for both Mohr-Coulomb and Drucker-Prager criteria in both 2D and 3D for the elastic ball radius of 230 mm. The Drucker-Prager model yielded higher loads at convergence than the Mohr-Coulomb model. However, both models gave similar results at the early stages of the simulations. It is important to mention here that for the 3D analyses cohesion was necessary in order to limit the tension zones.

A research studied by Wojciechowski (2018) demonstrated that the Drucker-Prager model generates a shear strength anywhere between 0.6 and 3 times that of the Mohr-Coulomb model. This is due to the Lode angle, which is a function of the intermediate stress. This means that in the present 3D simulations one of the following two conditions hold

$$\begin{aligned} \theta > \theta_0 \quad &\rightarrow \quad \sin(\phi') < \sqrt{3}\tan\left(-\frac{\theta+\theta_0}{2}\right) \\ \theta < \theta_0 \quad &\rightarrow \quad \sin(\phi') < \sqrt{3}\tan\left(-\frac{\theta+\theta_0}{2}\right) \end{aligned} \tag{14}$$

Where θ_0 and θ are respectively the Lode angle at failure and at the current state of stress. In the case of plain strain conditions, the Mohr-Coulomb and Drucker-Prager criterion are equivalent if the Poisson’s ratio in the plastic zones is taken as $\nu = 0.5$ and the Drucker-Prager parameters are established with $\theta_0 = 0$. This was not the case for the previously discussed 2D simulations. An example of the horizontal displacement field produced with the Drucker-Prager model is shown in Fig. 20. Also shown in Fig. 20 is the geostatic analysis that leads to these

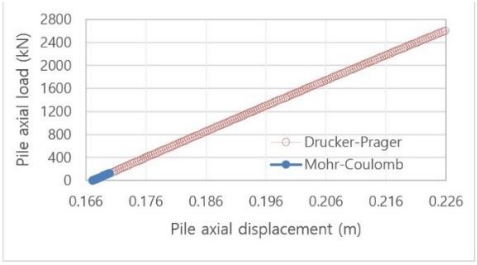

(a) Results of Drucker-Prager and Mohr-Coulomb criteria

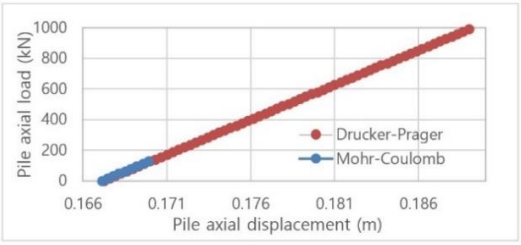

(b) A zoom of the Mohr-Coulomb zone

Fig. 19 Pile head axial load versus axial displacement resulting from the 3D FEM plasticity analyses

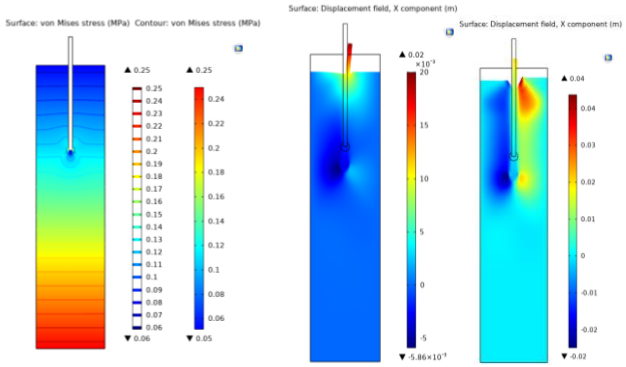

Geostatic analysis step P = 47.5 kN P_{max}= 180.6 kN

Fig. 20 FEM results of load control analysis in 2D using the Drucker-Prager criterion

horizontal displacements. These results were obtained by incrementing the axial load (load-control analysis) while applying a constant horizontal displacement of 20 mm (horizontal pile perturbation).

As depicted, for different intermediate and failure loads, the magnitudes of the horizontal displacements are the greatest in the soil region close to the surface in the direction of the applied perturbation. However, one can also observe that a tension zone is produced in the soil along the pile length opposite to this direction. For the Mohr-Coulomb model (Fig. 21), a similar behavior is observed for both intermediate and failure axial loads. All of these simulations were possible by elimination of the singularities via the introduction of an elastic or rigid ball at the pile tip. Without this modelling solution, one would have to assume a fictitious value of cohesion, which for a sand medium is unrealistic.

A 3D FEM simulation is necessary to model a pile having a channel cross section. This was not possible in the previous 2D simulations. These simulations were carried out using a ball of radius 230 mm from the center of the

Table 8 Pile axial load at failure from 3D FEM elasto-plastic analyses using the Drucker-Prager/Mohr-Coulomb criteria

Failure criterion	Drucker-Prager	Mohr-Coulomb
Maximum Axial Load (kN)	2838.4	125.5

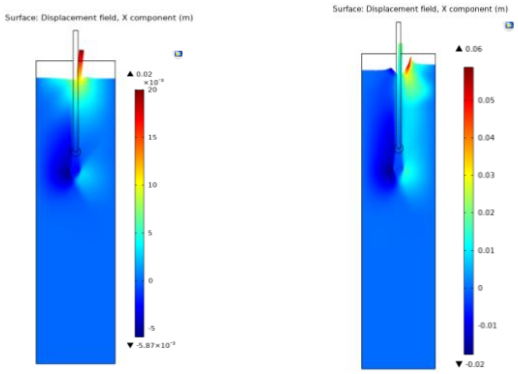

P = 47.5 kN P_{max}= 137.8 kN

Fig. 21 FEM results of load control analysis in 2D using the Mohr-Coulomb criterion

channel section with cohesion values of 2 kPa and 40 kPa applied for Drucker-Prager and Mohr-Coulomb criteria, respectively. An internal friction angle (φ') of 25 degrees was considered for numerical simulations using both criteria (Table 8). Fig. 22 shows the geostatic analysis as well the horizontal displacements of the soil-pile system at failure using the Drucker-Prager model. Moreover, in order to better assess the soil behavior, an image pertaining solely to soil displacements is also shown. Again, compression and tension zones are clearly discernible. Fig. 23 shows the results obtained with the Mohr-Coulomb once again indicating a similar behavior.

7. Validation of elasto-plastic analyses using field tests

The plasticity analyses were also carried out in the context of the field tests conducted by Comodromos *et al.* (2003). One must consider however that the plasticity parameters (Table 9) varied approximately with depth (layered soil). It is very difficult to obtain these parameters with certitude. Moreover, as expected, because of the tension stresses developed in the soil medium a ball was absolutely essential in order to obtain a converged solution. In this case, when comparing the axial load versus settlement curves (Fig. 24), the results are less satisfactory than for the previous non-linear elastic analyses. From the experience acquired in this study, the elasto-plastic analysis is more sensitive than the non-linear elastic one. For the elasto-plastic analyses the effect of both types of singularities, one linked to the high-tension zones and the other to the shape of the pile cross-section (re-entrant corners), play a greater role.

8. Conclusions

The present study examined the difficulties of modelling

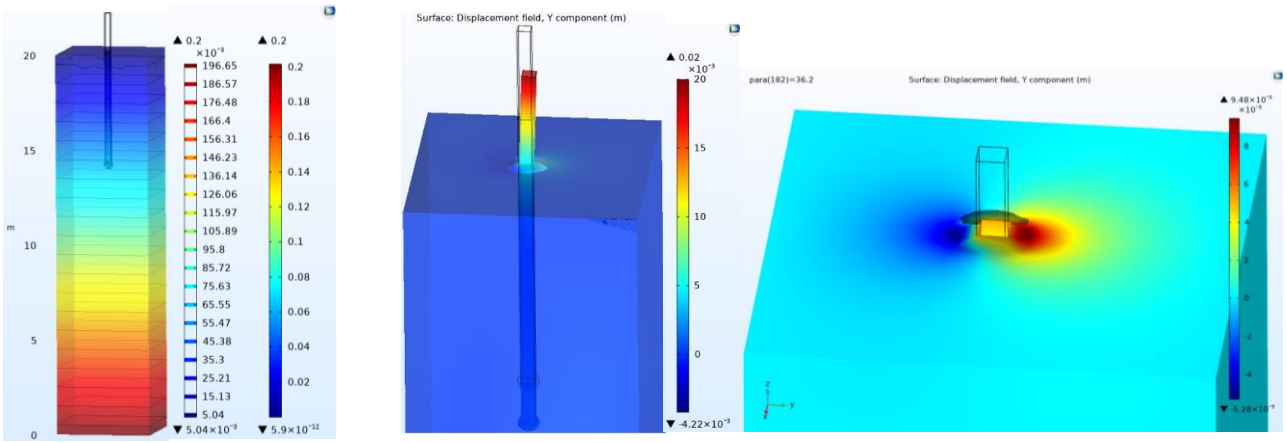

Geostatic analysis step

Pile displacement (P_{max} = 2838.4 kN)

Soil displacement (P_{max} = 2838.4 kN)

Fig. 22 FEM results of load control analysis in 3D using the Drucker-Prager criterion

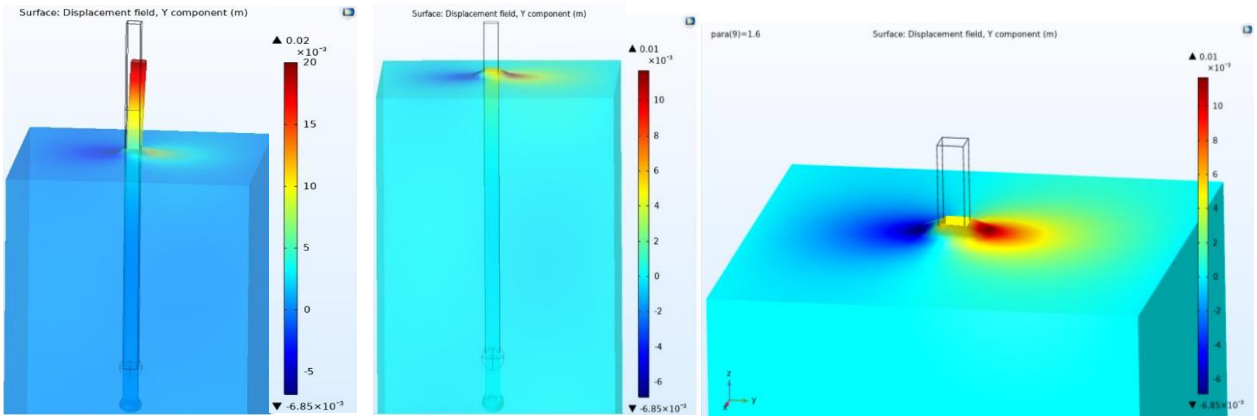

Pile displacement (P_{max} = 125.5 kN)

Soil displacement (P_{max} = 125.5 kN)

Fig. 23 FEM results of load control analysis in 3D using the Mohr-Coulomb criterion

a continuum that possesses inherent singularities. This problem, exemplified by the FEM calculations, also exposes the limitations of linear elastic theory when used to represent a granular soil medium. Generally, non-cemented granular materials do not resist tension. This fact renders the FEM analyses complicated from both the modellers' and numerical analysts' point of views. The study brought forth the suitability, notwithstanding the limitations previously discussed, of non-linear elastic soil models concerning a sand medium. This is justified if one considers that non-cemented sand is non-plastic. The two classic non-linear elastic soil models (Duncan-Chang and Hyperbolic) used in FEM model yielded, in general, similar results in both 2D and 3D. Some slight difference was observed in 3D but inconclusive from the practical engineering end. The Duncan-Chang and Hyperbolic soil models performed quite well when modelling a field test (Comodromos *et al*. 2003). The plasticity analyses induced a new modelling strategy in order to eliminate tension singularities. This was the introduction of a spherical elastic zone in the immediate vicinity of the pile tip. The Drucker-Prager model in general, yielded higher loads at convergence than the Mohr-Coulomb model in both 2D and 3D FEM analyses. In particular, both models gave similar results in the early stages of the simulations. It was also shown that for different intermediate and failure loads, the magnitudes of the horizontal displacements are the greatest in the soil region close to the surface in the direction of the applied perturbation. Simulations also yielded a tension zone in the soil along the pile length opposite to this direction. For the Mohr-Coulomb model, a similar behavior is observed for both intermediate and failure axial loads. All of these simulations were possible by elimination of the singularities via the introduction of an elastic or rigid ball at the pile tip. Without this modelling solution, one would have to assume a fictitious value of cohesion, which for a sand medium is unrealistic. A 3D FEM simulation is necessary to model a pile having a channel cross-section. This was not possible in the previous 2D simulations. Again, compression and tension zones are clearly discernible. These simulations

were carried out using a ball of radius 230 mm from the center of the channel section. Field tests confirm (Comodromos et al. 2003), at least in the context of this study, that non-linear elastic models are less sensitive to singularities.

Finally, based on the results of this study, non-linear elastic models are numerically less susceptible to convergence issues than plasticity models. More studies of this genre are required in order to better understand the intricacies related to numerical modelling of a pile-soil interaction.

Acknowledgments

The authors express their thanks to the civil engineering department at Laval University for their investment in the computational software and technical support of the hardware.

References

Alielahi, H. and Adampira, M. (2016), "Comparison between empirical and experimental ultimate bearing capacity of bored piles; a case study", *Arab. J. Geosci*., **9**(1), 16. https://doi.org/10.1007/s12517-015-2211-y.

Al-Soudani, W.H. and Albusoda, B.S. (2021), "An experimental study on bearing capacity of steel open ended pipe pile with exterior wings under compression load", *Geotech. Geol. Eng.*, **39**, 1299-1318. https://doi.org/10.1007/s10706-020-01559-0.

Bakroon, M., Daryaei, R., Aubram, D. and Rackwitz, F. (2019), "Numerical evaluation of buckling in steel pipe piles during vibratory installation", *Soil Dyn. Earthq. Eng.*, **122**, 327-336. https://doi.org/10.1016/j.soildyn.2018.08.003.

Broms, B.B. (1963), "Allowable bearing capacity of initially bent piles", *J. Soil Mech. Found. Div. (ASCE)*, **89**(5), 73-92.

Budhu, M. (2007), *Foundations and Earth Retaining Structures*, John Wiley & Sons, Tucson, Arizona, USA.

Budhu, M. (2010), *Soil Mechanics and Foundations*, John Wiley & Sons, Tucson, Arizona, USA.

Canadian Steel Handbook (2007), *Canadian Institute of Steel Construction (CISC)*, 9th Ed., 3rd rev. ISBN: 9780888111241, 088811124X.

Cheung, Y.K., Lee, P.K.K. and Zhao, W.B. (1991), "Elastoplastic analysis of soil-pile interaction", *Comput. Geotech.*, **12**(2), 115-132. https://doi.org/10.1016/0266-352x(91)90002-w.

Comodromos, E.M., Anagnostopoulos, C.T. and Georgiadi, M.K. (2003), "Numerical assessment of axial pile group response based on load test", *Comput. Geotech.*, **30**(6), 505-515. https://doi.org/10.1016/s0266-352x(03)00017-x.

Comodromos, E.M., Papadopoulou, M.C. and Rentzeperis, I.K. (2009), "Pile foundation analysis and design using experimental data and 3-D numerical analysis", *Comput. Geotech.*, **36**(5), 819-836. https://doi.org/10.1016/j.compgeo.2009.01.011.

COMSOL Multiphysics Reference Manual. (2018), Version 5.4., https://doc.comsol.com/5.4/doc/com.comsol.help.comsol/COMSOL_ProgrammingReferenceManual.pdf.

Deng, T., Liu, Q. and Huang, M. (2016), "Buckling of fully embedded single piles by using the modified Vlasov foundation model", *Int. J. Struct. Stab. Dyn.*, **17**(1), 1750007. https://doi.org/10.1142/s0219455417500079.

Desai, C.S. (1974), "Numerical design-analysis for piles in sands", *J. Geotech. Eng. Div. (ASCE)*, **100**(6), 613-635. https://doi.org/10.1016/0148-9062(74)91242-x.

Desai, C.S. and Holloway, D.M. (1972), "Load-deformation analysis of deep pile foundations", *Proceedings of the Symposium on Applications of the Finite Element Method in Geotechnical Engineering*, Vicksburg, Mississippi, May.

Drucker, D.C. and Prager, W. (1952), "Soil mechanics and plastic analysis or limit design", *J. Appl. Math.*, **10**(2), 157-165. https://doi.org/10.1090/qam/48291.

Duncan, J.M. and Chang, C.Y. (1970), "Nonlinear analysis of stress and strain in soils", *J. Soil Mech. Found. Div. (ASCE)*, **96**(5), 1629-1653.

Dunlop, P., Sandiford, R.E. and Erali, D.R. (1993), "Instrumented load test on a bent pile", *Proceedings of the 3rd International Conference on Case Histories in Geotechnical Engineering*, Rolla, Missouri, June.

Dusicka P., Itanib A.M. and Buckleb I.G. (2007), "Cyclic response of plate steels under large inelastic strains", *J. Constr. Steel Res.*, **63**, 156-164. https://doi.org/10.1016/j.jcsr.2006.03.006.

El Kamash, W. and El Naggar, H. (2018), "Numerical study on buckling of end-bearing piles in soft soil subjected to axial loads", *Geotech. Geol. Eng.*, **36**(5), 3183-3201. https://doi.org/10.1007/s10706-018-0529-4.

Eslami, A. and Fellenius, B.H. (1997), "Pile capacity by direct CPT and CPTu methods applied to 102 case histories", *Can. Geotech. J.*, **34**(6), 886-904. https://doi.org/10.1139/t97-056.

Fahey, M. and Carter, J.P. (1993), "A finite element study of the pressure-meter test in sand using non-linear elastic plastic model", *Can. Geotech. J.*, **30**(2), 348-362. https://doi.org/10.1139/t94-096.

Foriero, A. and Bayati, Z. (2018), "Three dimensional FEM buckling analyses of piles embedded in various soil types", *Struct. Integr. Life*, **18**(3), 171-179. UDC: 624.012.45.072.2.04: 519.673.

Foriero, A. (2004), "Notes de cours supplémentaires". *Introduction à la méthode des éléments finis*, Université Laval, Québec, Cours GCI-7030, 1-106.

Foriero, A. and Ladanyi, B. (1995), "FEM simulation of interface problem for laterally loaded piles in permafrost", *Cold Reg. Sci. Technol.*, **23**(2), 121-126. https://doi.org/10.1016/0165-232x(94)00008-l.

Foriero, A. and Ladanyi, B. (1991), "Generalized FEM algorithm for laterally loaded piles in permafrost", *Can. Geotech. J.*, **28**(4), 523-541. https://doi.org/10.1139/t91-069.

Foriero, A. and Ladanyi, B. (1990), "Finite element simulation of behaviour of laterally loaded piles in permafrost", *J. Geotech. Eng. (ASCE)*, **116**(2), 266-284. https://doi.org/10.1061/(asce)0733-9410(1990)116:2(266).

Glick, G.W. (1948), "Influence of soft ground on the design of long piles", *Proceedings of the 2nd International Conference on Soil Mechanics and Foundation Engineering*, Institution of Civil Engineers, London, June.

Hardin, B.O. and Drnevich, V.P. (1972), "Shear modulus and damping in soils: Design equations and curves", *J. Soil Mech. Found. Div. ASCE*, **98**(7), 667-692.

Hataf, N. and Shafaghat, A. (2015), "Numerical comparison of bearing capacity of tapered pile groups using 3D FEM", *Geomech. Eng.*, **9**(5), 547-567. https://doi.org/10.12989/gae.2015.9.5.547.

Heyman, J. (1972), *Coulomb's Memoir on Statics*, Cambridge University Press, Cambridge, UK.

Jaky, J. (1944), "The coefficient of earth pressure at rest", *J. Soc. Hungarian Architects Eng.*, **7**, 355-358.

Jeong, S., Ko, J., Won, J. and Lee, K. (2015), "Bearing capacity analysis of open-ended piles considering the degree of soil plugging", *Soils Found.*, **55**(5), 1001-1014. https://doi.org/10.1016/j.sandf.2015.06.007.

Jesmani, M., Nabavi, S.H. and Kamalzare, M. (2014), "Numerical

analysis of buckling behavior of concrete piles under axial load embedded in sand", *Arab J. Sci. Eng*., **39**(4), 2683-2693. https://doi.org/10.1007/s13369-014-0970-5.

Kondner, R.L. (1963), "Hyperbolic stress-strain response: cohesive soils", *J. Soil Mech. Found. Div. (ASCE)*, **89**(1), 115-143.

Kumar Khan, A. and Pise, P.J. (1997), "Dynamic behaviour of curved piles", *Comput. Struct*., **65**(6), 795-807. https://doi.org/10.1016/s0045-7949(97)00043-6.

Lee, J.H. and Salgado, R. (1999), "Determination of pile base resistance in sands", *J. Geotech. Geoenviron. Eng.*, **125**(8), 673-683. https://doi.org/10.1061/(asce)1090-0241(1999)125:8(673).

Nadeem, M., Chakraborty, T. and Matsagar, V. (2015), "Nonlinear buckling analysis of slender piles with geometric imperfections", *J. Geotech. Geoenviron. Eng.*, **141**(1), 06014014. https://doi.org/10.1061/(asce)gt.1943-5606.0001189.

Meyerhof, G.G. (1976), "Bearing capacity and settlement of pile foundations". *J. Geotech. Eng. Div. (ASCE)*, **102**(3), 195-228.

Owen, D.R.J. and Hinton, E. (1986), *Finite Elements in Plasticity: Theory and Practice*, Pine ridge Press Limited, Swansea, Wales, UK.

Paik, K., Lee, J. and Kim, D. (2011), "Axial response and bearing capacity of tapered piles in sandy soil", *Geotech. Test. J*., **34**(2), 122-130. https://doi.org/10.1520/gtj102761.

Ramirez-Henao, A.F. and Paul Smith-Pardo, J. (2015), "Elastic stability of pile-supported wharves and piers", *Eng. Struct.*, **97**, 140-151. https://doi.org/10.1016/j.engstruct.2015.04.007.

Ren, Q.X., Hou, C., Lam, D. and Han, L.H. (2014), "Experiments on the bearing capacity of tapered concrete filled double skin steel tubular (CFDST) stub columns", *Steel Compos. Struct.*, **17**(5), 667-686. https://doi.org/10.12989/scs.2014.17.5.667.

Rezaiee, M.P. and Mazindrani, Z.H. (1990), "Optimal capacity of axially loaded bent pile", *Amirkabir J. Sci. Technol*., **4**(15), 65-78.

Shields, D.R. (2007), "Buckling of micropiles", *J. Geotech. Geoenviron. Eng.*, **133**(3), 334-337. https://doi.org/10.1061/(asce)1090-0241(2007)133:3(334).

Singularities (2015), Singularities in Finite Element Models: Dealing with Red Spots; *COMSOL Blog*, https://www.comsol.com/blogs/singularities-in-finite-element-models-dealing-with-red-spots/.

Tomlinson, M. and Woodward, J. (2014), *Pile Design and Construction Practice*, CRC Press, Taylor & Francis Group, London, UK.

Trochanis, A.M., Bielak, J. and Christiano, P.P. (1991), "Three-dimensional nonlinear study of piles", *J. Geotech. Eng. ASCE*, **117**(3), 429-447. https://doi.org/10.1061/(asce)0733-9410(1991)117:3(429).

Veiskarami, M., Eslami, A. and Kumar, J. (2011), "End-bearing capacity of driven piles in sand using the stress characteristics method: analysis and implementation", *Can. Geotech. J*., **48**(10), 1570-1586. https://doi.org/10.1139/t11-057.

Wojciechowski, M. (2018), "A note on the differences between Drucker-Prager and Mohr-Coulomb shear strength criteria", *Studia Geotech. et Mech.*, **40**(3), 163-169. https://doi.org/10.2478/sgem-2018-0016.

Wood, D.M. (2007), *Soil Behaviour and Critical State Soil Mechanics*, Cambridge University Press, Cambridge, UK.

Zhang, X., Tang, L., Ling, X. and Chan, A. (2020), "Critical buckling load of pile in liquefied soil", *Soil Dyn. Earthq. Eng*., **135**, 106197. https://doi.org/10.1016/j.soildyn.2020.106197.